www.advnanobiomedres.com

Silk Fibroin Particles as Carriers in the Development of Hemoglobin-Based Oxygen Carriers

Marisa O. Pacheco, Henry M. Lutz, Jostin Armada, Nickolas Davies, Isabelle K. Gerzenshtein, Alaura S. Cakley, Bruce D. Spiess, and Whitney L. Stoppel*

Oxygen therapeutics has a range of applications in transfusion medicine and disease treatment. Synthetic molecules and all-natural or semisynthetic hemoglobin-based oxygen carriers (HBOCs) have seen success as potential circulating oxygen carriers. However, many early HBOC products stalled in development due to side effects from excess hemoglobin in the blood stream and hemoglobin entering the tissue. To overcome these issues, research has focused on increasing the molecular diameter of hemoglobin by polymerizing hemoglobin molecules or encapsulating hemoglobin in liposomal carriers. This work leverages the properties of silk fibroin, a cytocompatible and nonthrombogenic biopolymer, known to entrap protein-based cargo, to engineer a fully protein-based oxygen carrier. Herein, an all-aqueous solvent evaporation technique is used to form silk particles via phase separation from a bulk polyvinyl alcohol phase. Particle size is tuned, and particles are formed with and without hemoglobin. The encapsulation efficiency and ferrous state of hemoglobin are analyzed, resulting in 60% encapsulation efficiency and a maximum of 20% ferric hemoglobin, yielding 100 µg mL⁻¹ active hemoglobin in certain silk fibroin-HBOCs formulations. The system does not elicit a strong inflammation response in vitro, demonstrating the potential for this particle system to serve as an injectable HBOC.

1. Introduction

Many injuries and diseases lead to local tissue hypoxia and/or systemic hypoxemia, with both acute and chronic diagnoses. Causes or comorbidities include, but are not limited to, traumatic injury, sickle cell disease, diabetes, COVID-19, kidney disease, stroke, and other hematologic conditions.^[1–5] One treatment strategy is respiratory supplementation of oxygen to better

saturate native red blood cells (RBCs). Another strategy is transfusing donated blood or blood components to improve oxygen carrying capacity. systemic Maintaining a blood supply for treatment of diseases or conditions resulting in low oxygen tension remains a critical challenge. Blood transfusion and blood product supply chain issues result from factors such as the limited shelf-life of stored RBC units, [6,7] spikes in demand due to seasonal^[8,9] or emergency surges,^[10,11] and breakdown of the supply chain, [12] motivating the need to develop alternatives to RBC transfusions that can overcome these dynamic challenges. The developed replacement ideally should replicate the oxygen carrying function of RBCs effectively and safely, with focus on pathogenfree and universally compatible solutions that can overcome transportation and storage limitations (see Ref. [13] for a recent perspective on this topic).

Over the past several decades, many materials including synthetic perfluorocarbons and hemoglobin-based oxygen

carriers (HBOCs) based on human,^[14] bovine,^[15–17] and recombinant hemoglobin^[18] have seen success. Some formulations such as HBOC-201, a bovine HBOC, achieved clinical approval in countries like South Africa, and advanced to late-stage clinical trials in the United States.^[16] However, early HBOCs were found to cause severe side effects as a function of two main factors. First, it was determined that particle extravasations into the tissue space through the vessel wall (fenestration diameter

M. O. Pacheco, H. M. Lutz, J. Armada, A. S. Cakley, W. L. Stoppel Departmentof Chemical Engineering University of Florida Gainesville, FL 32611, USA E-mail: whitney.stoppel@ufl.edu

The ORCID identification number(s) for the author(s) of this article can be found under https://doi.org/10.1002/anbr.202300019.

© 2023 The Authors. Advanced NanoBiomed Research published by Wiley-VCH GmbH. This is an open access article under the terms of the Creative Commons Attribution License, which permits use, distribution and reproduction in any medium, provided the original work is properly cited.

DOI: 10.1002/anbr.202300019

N. Davies, B. D. Spiess Department of Anesthesiology College of Medicine University of Florida Gainesville, FL 32611, USA

I. K. Gerzenshtein Department of Microbiology and Cell Science University of Florida Gainesville, FL 32611, USA

W. L. Stoppel J. Crayton Pruitt Family Department of Biomedical Engineering University of Florida Gainesville, FL 32611, USA



www.advancedsciencenews.com www.advnanobiomedres.com

ADVANCED NANOBIOMED RESEARCH

 $\approx\!50\text{--}100~\text{nm}^{[19]}\!)$ caused scavenging of nitric oxide (NO), leading to systemic hypertension and oxidative tissue injury. [20] Second, excess cell-free hemoglobin present in circulation overwhelmed the native clearance processes executed by macrophages in the liver and spleen, leading to renal toxicity. [21] To address these challenges, strategies to increase the molecular diameter of the HBOC and limit free hemoglobin in circulation have become requirements in the design of modern HBOCs. These strategies include chemical cross-linking of hemoglobin, [22,23] polymerization of hemoglobins, [24-26] and encapsulation of hemoglobin in liposome and nano- and microparticle systems. [27,28] Liposome encapsulated hemoglobin's have demonstrated many of the desired design criteria for an alternative oxygen carrier, including an absence of blood group antigens and blood-borne pathogens, and a prolonged storage capacity. [29-31]

While liposome encapsulated systems show great potential for the eventual translation of new oxygen carrier technologies, several challenges still exist in the field. One challenge is obtaining dispersions of particles or carriers with similar hemoglobin concentrations to native RBCs (\approx 35 g dL⁻¹). In liposome systems, work has been able to achieve Hb concentrations near $15\,g\,dL^{-1}.^{[32]}$ Recently, researchers are investigating novel techniques to maximize loading such as utilizing metal organic frameworks, [33] protein systems, [34] and microgelmaterials.[35]In this study, we evaluate the encapsulation of hemoglobin in a silk fibroin particle system with the goal of limiting potential costs of production and storage, with a focus on naturally derived materials that are stable over long-time periods at room temperature or under simple refrigeration with adequate hemoglobin loading (4°C, see Supplemental Figure S1, Supporting Information).[36-38] Silk fibroin is a biopolymer isolated from the cocoons of Bombyx mori silkworms and in formats such as films, has demonstrated effective encapsulation and stabilization of large, bioactive proteins and other blood components^[39,40] as well as biocompatible and antithrombogenic behavior. [41,42] Studies suggest that the semicrystalline nature of the silk fibroin protein can be leveraged to stabilize the structure of proteins^[43] that are entrapped within the crystal structure of the β -sheet domains present in the heavy chain of silk fibroin. Utilizing this hydrophobic collapse of the silk fibroin protein allows for addition of these bioactive components in the soluble state, but stabilization in both hydrated and dry (lyophilized) states are possible (see reference for a deeper review). [40]

Bioactive molecule encapsulation and stability in silk fibroin nano- and microparticles has previously been investigated in the context of cancer nanomedicines and potential intraperitoneal delivery. [44–48] Due to the nature of anticancer drugs being mainly small molecules and the complexity in studying natural biopolymer and small molecule interaction in a crystallized state, there is limited knowledge of how silk particle systems encapsulate and stabilize larger protein-based cargo. We also seek to understand if stabilization in the nano- or microparticle systems differs from the β -sheet crystalline driven process observed in macro-sized silk materials such as films and scaffolds. [40,49] Additionally, the most common method of synthesis for silk-based anticancer nanomedicines is organic solvent desolvation, [30] which would potentially cause oxidative damage to hemoglobin cargo, as seen with some HBOC synthesis methods, which prompted shifts and eventual

optimization of formulations and protocols^[30] to achieve high levels of encapsulation and minimal hemoglobin damage.

Thus, we look to take advantage of the ability of silk fibroin biopolymers to stabilize protein cargo while leveraging an all-aqueous particle fabrication technique inspired by the synthesis of silk nanoporous films.^[50,51] In this work, we encapsulate human hemoglobin in silk fibroin nano- and microparticles, focusing on the characterization of the parameter space available for making these particles with a focus on reproducibility, hemoglobin structure, and loading efficiency. We aim to form nanoparticle formulations with a size distribution between 200-700 nm, with all nanoparticles being larger than 100 nm to avoid the potential for extravasations through the vessel wall. An ideal formulation would minimize the variability in particle size and show high reproducibility from batch to batch. To evaluate the potential for silk fibroin nanoparticles to stabilize and carry hemoglobin, we characterize the size, crystalline character, and internal morphology of four separate formulations chosen to modulate particle size. We then evaluate the passive encapsulation of hemoglobin at two concentrations in the same particle formulations. Last, we assess the cell-material interaction of our silk fibroin-hemoglobin-oxygen carrier (sfHBOC) system with macrophage-like cells in vitro to better understand the potential safety and clearance of the sfHBOCs.

2. Results and Discussion

Encapsulation of hemoglobin in an all-natural protein carrier that ensures maintenance of hemoglobin structure and function within the biopolymer network has the potential to address current challenges in the field of hemoglobin-based oxygen carriers. In this work, we utilize silk fibroin proteins isolated from *Bombyx* mori silkworm cocoons as the stabilizing biopolymer and carrier system. We approach this development of a silk fibroin hemoglobin-based oxygen carrier holistically, first characterizing the silk fibroin polymer solution itself and ending with the encapsulation of hemoglobin in the created nanoparticle system and its interaction with macrophage-like cells in vitro. Initial experiments evaluating formulation parameters for size and morphology were completed with a bovine hemoglobin solution of primarily methemoglobin (non-O2 binding Hb, denoted as mHb), but subsequent experiments assessing binding of O2 and cell response utilized HbA₀, a nonglycated, ferrous form of hemoglobin (Millipore Sigma, H0267). sfHBOCs are formed using an all-aqueous method where the silk biopolymer is phase separated and crystallized using a bulk solution of 5% polyvinyl alcohol. We start by characterizing the neat silk particle parameter space before introducing hemoglobin and forming sfHBOCs (Table 1).

2.1. Organic Solvent-Free Methods Yield Silk Particles in Size Range of Current HBOCs

2.1.1. Extraction Time Yields Control of Precursor Silk Polymer Solution Molecular Weight Ranges

In order to reduce variability in sfHBOC particle size, robust control over and reduction of variation in biopolymer molecular weight is needed. In the silk fibroin biomaterials field, it is well

ADVANCED NANOBIOMEI RESEARCH

www.advancedsciencenews.com www.advnanobiomedres.com

Table 1. Formulation name, associated symbol, and details for particle formations used throughout studies presented in this manuscript.

Formulation Name	Symbol	Silk Extraction		Silk Concentration		Hemoglobin Concentration	
		Time [min]		[% w/v]		[µg mL ⁻¹]	
60 min-1.00%-0 Hb	•	60	closed	1.00	circle	0	purple
60 min-0.25%-0 Hb	•	60	closed	0.25	triangle	0	purple
90 min-1.00%-0 Hb	0	90	open	1.00	circle	0	purple
90 min-0.25%-0 Hb	Δ	90	open	0.25	triangle	0	purple
60 min-1.00%-125 Ht	•	60	closed	1.00	circle	125	pink
60 min-0.25%-025 Hb	A	60	closed	0.25	triangle	125	pink
90 min-1.00%-125 Hb	0	90	open	1.00	circle	125	pink
90 min-0.25%-125 Hb	Δ .	90	open	0.25	triangle	125	pink
60 min-1.00%-250 Hb	•	60	closed	1.00	circle	250	red
60 min-0.25%-250 Hb	A	60	closed	0.25	triangle	250	red
90 min-1.00%-250 Hb	0	90	open	1.00	circle	250	red
90 min-0.25%-250 Hb	Δ .	90	open	0.25	triangle	250	red

understood that the extraction time of the fibroin polymer impacts the final material properties regardless of material format, with trends in extraction time (15, 30, and 60 min) being

inversely proportional to biopolymer molecular weight.^[52] Thus, we hypothesized that longer extraction times would not only lead to shorter average fibroin chain lengths, but also a less variable polymer solution. Using sodium dodecyl sulfatepolyacrylamide gel electrophoresis (SDS-PAGE, Figure S1, Supporting Information), we measured silk fibroin molecular weights and confirmed trends in published literature^[52,53] as shown in Figure 1A. We determined that 90 min extraction times yielded the most uniform polymer solutions with the lowest molecular weights, compared to 15, 30, and 60 min of extraction (Figure 1B, S1, Supporting Information). Moving forward, we will use the 60 and 90 min extracted silk fibroin solutions for particle formulations. The 60 min extracted solutions had a median molecular weight of 125 ± 3 kilodaltons (kDa) while the 90 min extracted solutions had a median molecular weight of $90 \pm 1 \,\mathrm{kDa}$. We determined that the silk fibroin polymer chain lengths are heterogenous as shown by determination of effective interquartile ranges (IQRs) for these silk solutions (Figure 1A, S1, Supporting Information). We calculated an IQR of \approx 95–105 kDa for 60 min of extraction versus an IQR of \approx 60–65 kDa for 90 min of extraction. While this heterogeneity in the biopolymer solutions exists, we wanted to confirm that the heterogeneity was consistent from batch to batch in terms of both the median molecular weight and level of heterogeneity. To test our hypothesis, we analyzed four separate 60 min extractions and found that the polymer chain length and distribution were

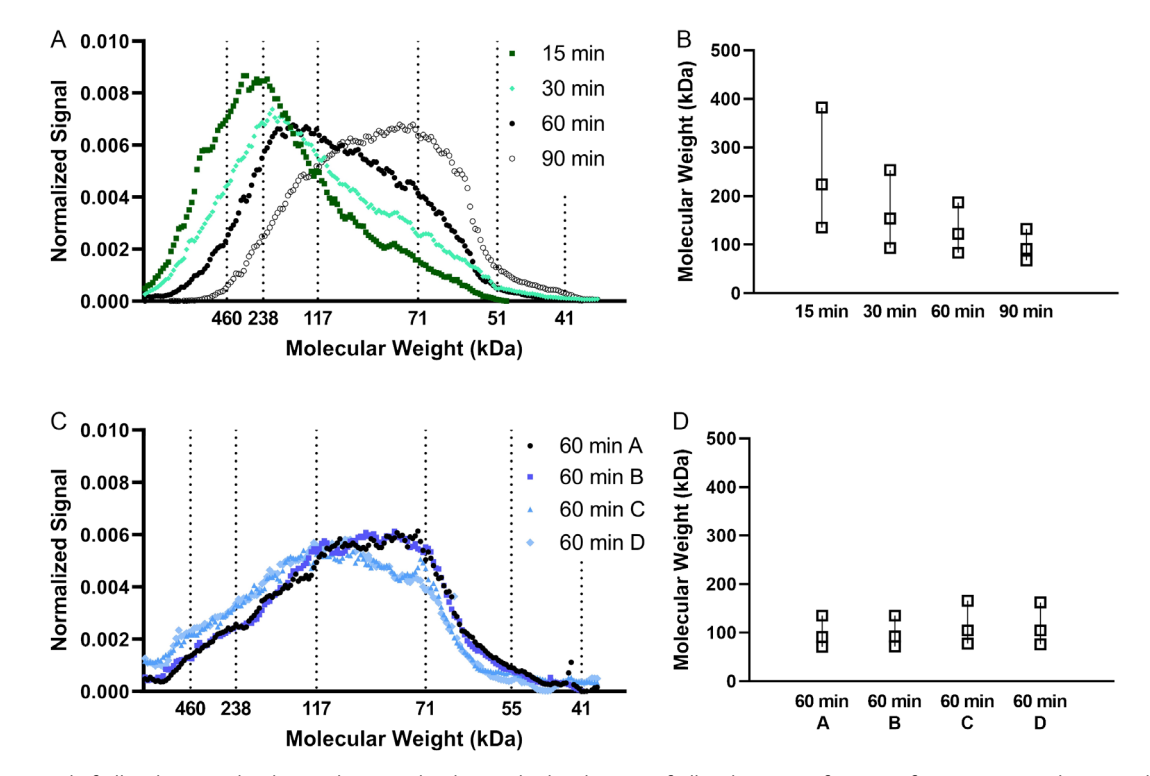


Figure 1. Control of silk polymer molecular weight. A) Molecular weight distributions of silk polymer as a function of extraction time determined by analysis of SDS-PAGE gels. 2 µg of silk polymer was loaded in each lane of a 7% Tris-acetate gel under reducing conditions. Densiometric analysis of colloidal blue stained gels yield the molecular weight distribution shown. B) Effective interquartile range (IQR) of silk molecular weight as a function of extraction time. Square data points represent the molecular weights at which the area under the distribution curve is equal to 25%, 50%, 75% of the total area. C) Molecular weight distributions of four batches of silk polymer solution that was extracted for 60 min determined by SDS-PAGE. Densiometric analysis of colloidal blue stained gels yields the molecular weight distribution shown. D) Effective interquartile range (IQR) of silk molecular weight as a function of batch. Square data points represent the molecular weights at which the area under the distribution curve is equal to 25%, 50%, 75% of the total area.

ADVANCED NANOBIOMEI RESEARCH

www.advancedsciencenews.com www.advnanobiomedres.com

consistent from batch to batch as analyzed in Figure 1C,D. Taken together, the results suggest that making silk particles with 90 min extracted silk may lead to smaller and more uniform particle distributions.

2.1.2. Decreased Silk Molecular Weight and Concentration Yields Smaller Particles

For applications in delivery of hemoglobin via systemic injection of sfHBOCs into the blood, particles in the range of 200 nm-1 µm are desired. [13] In addition, for these particle systems to be applicable in a clinical setting, control over both particle size and distribution is required. Given that the 90 min extracted silk fibroin solution has the lowest distribution of molecular weights, we hypothesized that utilizing 90 min extracted silk fibroin solution in an all-aqueous silk particle fabrication method^[50,51] would yield smaller and more monodisperse silk particles in solution. In addition, we recognize that the level of biopolymer entanglement during the phase separation process will dictate the theoretical number of polymers present in each particle and that previous work demonstrates the impact of polymer concentration on particle size. [54,55] Thus. we hypothesized that lower silk concentrations and lower silk molecular weights would lead to fewer secondary structure interpolymer interactions, resulting in decreased average silk particle size.

To determine the extent to which molecular weight and concentration impact particle size, we quantified particle hydrodynamic diameters using dynamic light scattering (DLS, Figure 2A,B) and confirmed results with scanning electron microscopy (SEM, Figure 2C-F). We compared particle formulations using 60 and 90 min extracted silk fibroin at concentrations of 1% w/v and 0.25% w/v (Figure 2A). Results show that extraction time, or the median molecular weight, is most impactful in dictating particle size. Particles formed at the two extremes, given by 1% w/v 60 min extracted silk (60 min-1%-0 mHb, $D_{\rm H} = 490 \pm 70 \,\mathrm{nm}$) and 0.25% w/v 90 min extracted silk (90 min-0.25%-0 mHb, $D_{\rm H} = 301 \pm 33$ nm) are statistically different ($p \le 0.01$) (see Table 1 for all formulation descriptions). The 90 min-0.25%-0 mHb formulation maintains this statistical difference from the other evaluated formulations (p < 0.01, Figure 2A). It is important to note that the reported $D_{\rm H}$ is the intensity weighted average hydrodynamic diameter determined by DLS, which can be inaccurate in the case of large, polydisperse samples. We performed additional analyses looking at the full intensity distribution functions and autocorrelation functions (Figure S2B-E, Supporting Information). Additionally, we calculated the difference between the intensity weighted average $D_{\rm H}$ and the hydrodynamic diameter that gives the maximum intensity (Figure S2A, Supporting Information). In normal distributions with low to moderate polydispersity we expect this difference to be small, and we determined this was true for 90 min formulations (Figure S2A, Supporting Information). This led us to focus our analysis to the 90 min formulations. In an assessment of dispersity, we calculated the full peak width at 68% (Figure 2B). We determined that lower concentrations led to tighter distributions, though the difference was not statistically significant. Qualitatively, SEM micrographs show that particle size decreases with decreasing biopolymer molecular weight, with quite observable differences at the extremes (Figure 2C compared to Figure 2F). Additionally, SEM micrographs confirm the polydispersity we expected in the 60 min conditions (Figure 2C,D). Our results agree with those found in the literature that modulation of silk particle size can be achieved using polymer concentration and molecular weight in the context of different fabrication strategies, such as microfluidic devices and organic solvent desolvation. [42,44,56,57]

To further assess structural changes in particles formed with different formulations, we analyzed crystalline content and internal particle structure using Fourier transform infrared (FTIR) spectroscopy and nanoscale computed tomography (Nano-CT), respectively. FTIR spectra can be compared to assess relative changes in crystalline content across formulations. This is done by deconvoluting the peak in the Amide I region,[58] shown in Figure 3A. The deconvolution allows for the determination of relative amounts of secondary protein structures present in the silk particles (Figure S3, Supporting Information) and β-sheet or crystalline content is reported in Figure 3B. Results show silk concentrations impact total crystalline content, with a two-way ANOVA showing the variable of silk concentration is significant (p = 0.0071). However, pairwise comparisons showed no significance with average β-sheet content being around 30%–40% in the formulations of interest (Figure 3B). High levels of crystalline content in our particle system is important for two reasons: 1) stable particles are formed by a hydrophobic collapse process, indicating that β -sheet crystalline structures should be present, $^{[57,59,60]}$ and 2) bioactive molecule stabilization is expected to be achieved by kinetically trapping the molecules in crystalline structures. [40] Thus we hypothesized that hemoglobin containing formulations would show a marked increase in helical content and a related drop in comparative crystalline content; this was confirmed using FTIR (Figure S5, Supporting Information). Thus, the consistency in high levels of crystalline content found in our particles is desirable for future applications, as the stabilization of the bioactive molecule, in this case hemoglobin, will be theoretically achieved evenly across formulations using 90 min extracted silk.

2.1.3. Discussion of the Role of Crystallinity in Protein Encapsulation

As such, β -sheet or crystalline content of the particles is critical for understanding the potential to include and stabilize hemoglobin within these particles to create sfHBOCs. As previously hypothesized, [40] proteins and biomolecules are stabilized within the crystalline domains of the silk protein, trapping the bioactive molecule, in this case hemoglobin, in a stable confirmation even when the particles experience various hydration levels or temperatures. This feature of silk fibroin biomaterials is what makes this all-natural carrier system advantageous as a HBOC. It is important to recognize that FTIR spectra are representative of a combined particle population and cannot give information at the resolution of a single particle. Given that the bulk analysis of FTIR spectra did not identify significant differences in crystalline content, we further explored the internal structure of the silk particles to better understand the regions of potential hemoglobin incorporation. Due to the resolution of the Nano-CT, only

2699307, 2023, 9, Downloaded from https://onlinelibrary.wiley.com/doi/10.1002/anbr.202300019 by University Of Florida, Wiley Online Library on [11/04/2024]. See the Terms and Conditions (https://onlinelibrary.wiley.

and-conditions) on Wiley Online Library for rules of use; OA articles are governed by the applicable Creative Commons License

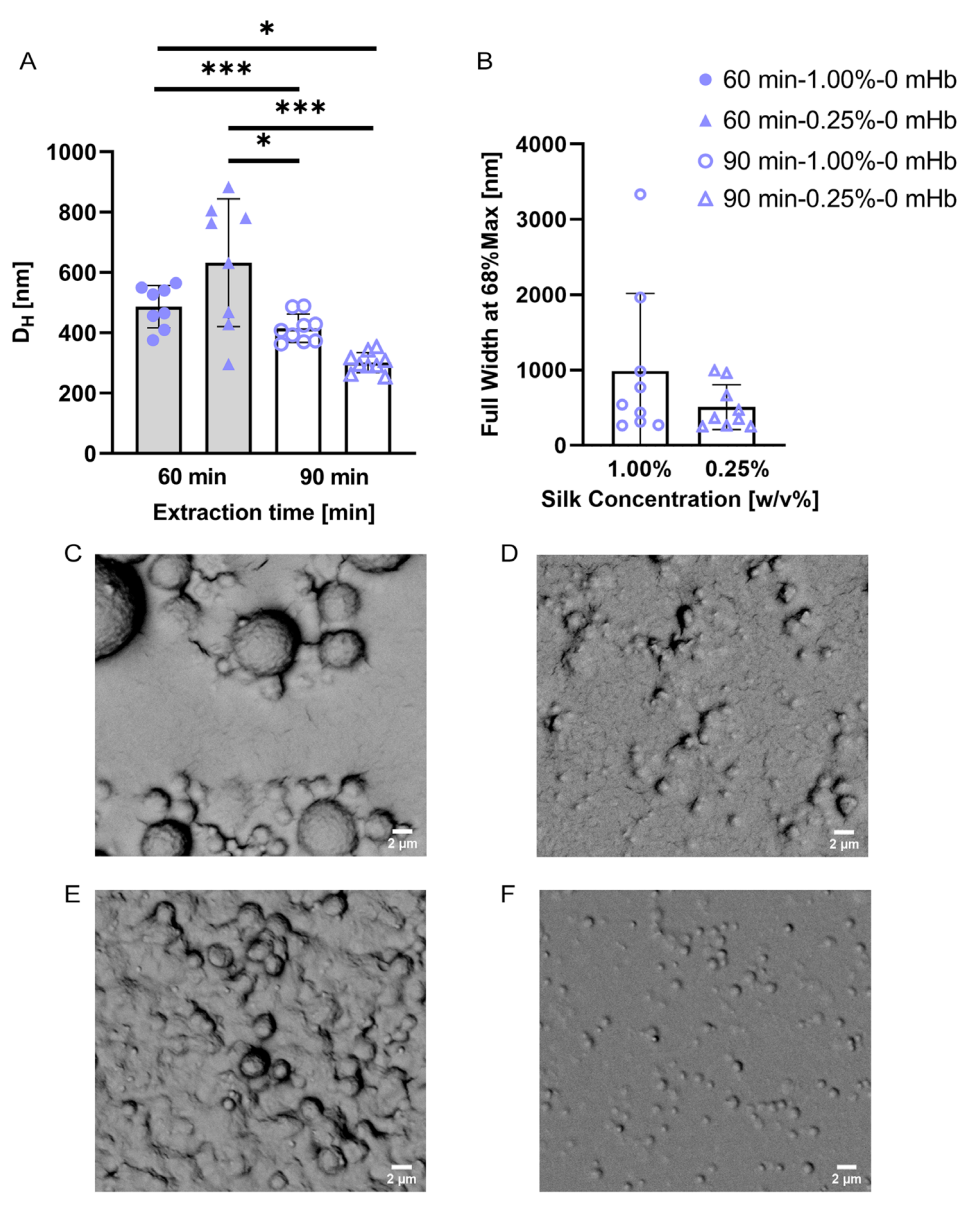


Figure 2. Silk molecular weight modulates particle size. A) Comparison of hydrodynamic diameter ($D_{\rm H}$) for all silk only formulations as measured by DLS. B) Comparison of peak width at 68% of the maximum, an assessment of dispersity. C) Representative SEM micrograph for 60 min-1%-0 mHb. D) Representative SEM micrograph for 90 min-1%-0 mHb. F) Representative SEM micrograph for 90 min-0.25%-0 mHb. It should be noted that the average silk particle hydrodynamic diameter is measured in a hydrated state, while SEM micrographs are captured after particles have been dried, and thus diameters estimated from SEM micrographs will not necessarily align with those determined by DLS. Data represented as AVG \pm SD ($n \ge 8$). A two-way ANOVA with Tukey post hoc testing was performed. Statistical significance is shown as * $p \le 0.05$, ** $p \le 0.01$, **** $p \le 0.001$, **** $p \le 0.001$, **** $p \le 0.001$, ***** $p \le 0.0001$.

particles on the micron scale can be adequately analyzed. Analysis of 10+ particles, $\approx 5-15 \, \mu m$ in diameter, showed that the particles contained a denser wall structure with an inner spongy core (Figure 3C). The particles maintained a consistent wall thickness of $2 \, \mu m$, suggesting that submicron particles are predominately dense polymer materials without a spongy core.

Together, results show that these formulations yield solid semicrystalline particles (Figure 3D,E). The Nano-CT and FTIR results suggest that hemoglobin has the potential to be incorporated into the crystalline regions present throughout

the particle, but that more hemoglobin may be captured in the denser outer wall due to changes in relative polymer density in particles larger than 2 μ m (outside the target size range of sfHBOC's) (Figure S4, Supporting Information). Taken with the particle size results (Figure 2A,F), this suggests that particles formed with 90 min extracted silk at 0.25% w/v will be predominantly dense polymeric particles without a distinct core. Thus, moving forward, we will only evaluate hemoglobin incorporation in this formulation (90 min-0.25%-X Hb) given the homogeneity along the radial direction in silk structure.

conditions) on Wiley Online Library for rules of use; OA articles are governed by the applicable Creative Commons License

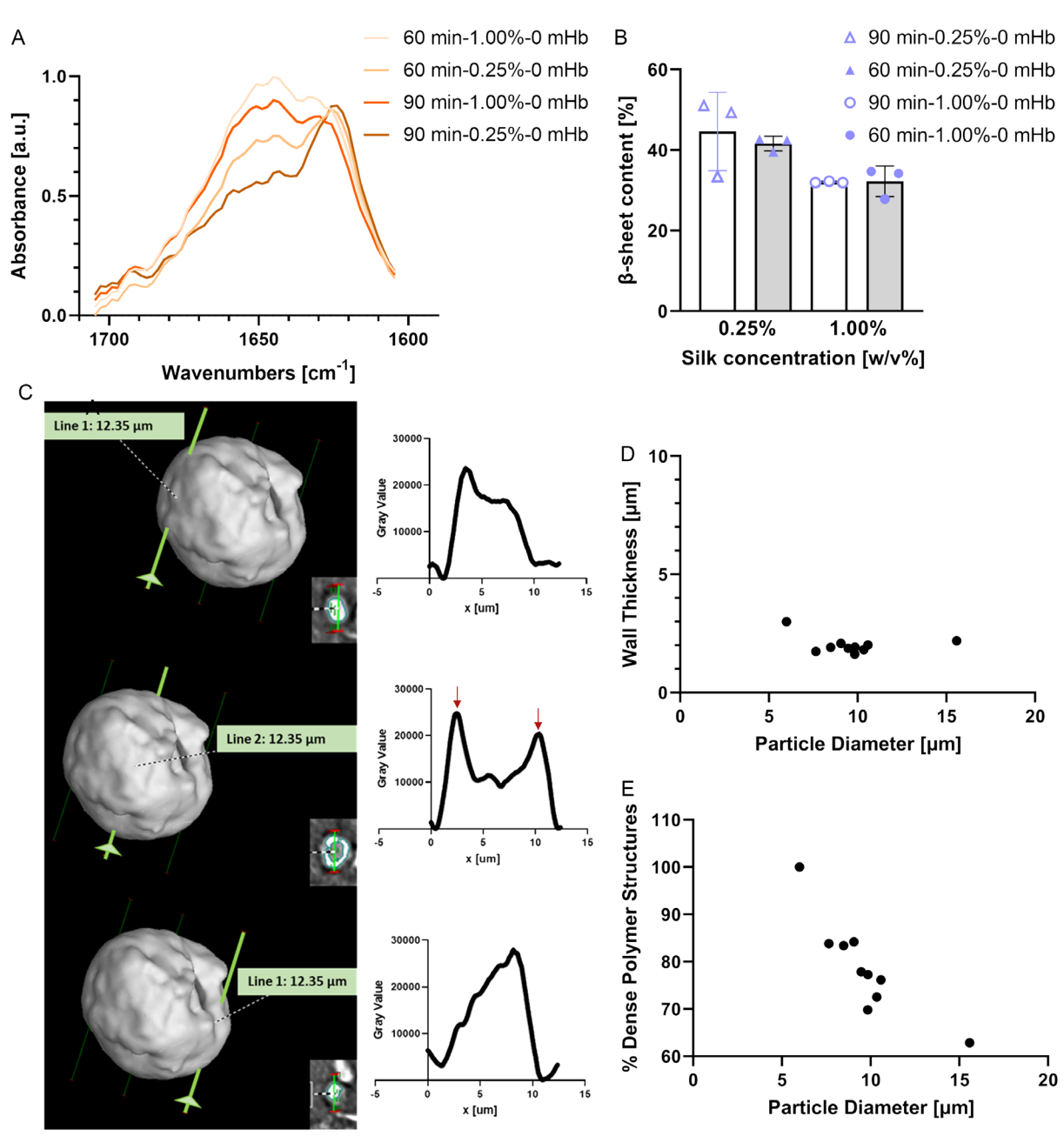


Figure 3. Highly crystalline domains are present across neat silk particle formulations. A) FTIR spectra of the Amide I region for all neat silk formulations. Samples were dried and FTIR spectra were collected using a micro attenuated total reflections technique. B) Following deconvolution of the Amide I peak following published methods, [58] relative level of β -sheet crystallinity was determined. Data are represented as AVG \pm SD (n=3). A two-way ANOVA with Tukey post hoc testing was performed. Statistical significance is shown as, $*p \le 0.05$, $**p \le 0.01$, $***p \le 0.001$, $****p \le 0.0001$. C) Nano-CT was performed to observe if differences in crystallinity or polymer density could be observed within a single particle. Shown is a 3D reconstruction of a silk microparticle. Line profiles of the gray value from 3 2D Nano-CT slices (inset) for each green line are shown to the right. Blue arrows indicate dense wall structures. D) Quantification of dense wall thickness via Nano-CT, shown is the thickness of the wall as a function of particle diameter for 10 particles imaged with Nano-CT. E) The calculated percent of dense volume in a particle as a function of diameter assuming the particle is a sphere.

2.2. Introducing Hemoglobin to Silk Fibroin Nanoparticles

Knowing that using aqueous solvent evaporation, silk particles can be formed in our target size range and that there is a substantial presence of β-sheet structures, we hypothesized that bioactive components such as hemoglobin could be kinetically

trapped in silk secondary structures. This can be achieved by introducing the component to the silk prior to the hydrophobic collapse and structural formation of the biomaterial. This strategy for passive incorporation and stabilization of bioactive molecules and proteins has been investigated and reported previously for a variety of silk fibroin-based materials that contain



www.advancedsciencenews.com www.advnanobiomedres.com

 β -sheet structures. [49,61–63] However, it is critical to confirm three main properties of our particle system with the introduction of hemoglobin: 1) limited change in size or polydispersity of the particles so that the neat silk fibroin particles are able to act as controls for future work; 2) the spatial orientation of hemoglobin allow for better understanding of intraparticle homogeneity; and 3) the amount of incorporated hemoglobin that remains active and able to bind and release oxygen. To assess changes in particle size, morphology, and dispersity, we incorporate a ferric (nonoxygen binding) form of hemoglobin termed methemoglobin (mHb). We perform DLS and SEM in order to understand how addition of the mHb protein impacts the particle properties.

2.2.1. Passive Encapsulation of Hemoglobin Increases Particles Size, But Maintains Similar Polydispersity

With the addition of hemoglobin, at either 125 or 250 µg of hemoglobin mL⁻¹ of silk-PVA solution, particle size increases by 100-150 nm, taking average particle size of the 90 min extracted silk at 0.25% w/v silk solution from \approx 300 to ≈400 nm (Figure 4A). However, the polydispersity of these formulations improved with the inclusion of mHb as shown by the peak width (Figure 4B). Taken together, Figure 4A,B show that even though average particle size is increasing, the dispersity is such that for all initial mHb concentrations, there is significant overlap in the size of particles present. For neat silk particles, the peak range given by the 68% maximum is 50-550 nm with an average of 300 nm, and for the $250 \,\mu g \, mL^{-1}$ of HbA₀ included, this shifts to a 250-650 nm range with a 450 average. This indicates that while we lose some of the smallest diameter particles from the population, there is still substantial overlap in the particle size for the tested formulations. These findings are also supported by the SEM micrographs for the respective conditions which show persistence of similarly sized particles across initial mHb concentrations (Figure 4C,D,E). As the hemoglobin concentration approaches levels similar to the silk, we do observe some amorphous polymers not participating in particle selfassembly surrounding normally formed particles (Figure 4E). We hypothesize that the increased hemoglobin concentration can disrupt the hydrophobic collapse of silk. We expect that this material is easily removed via filtration since it was not visible in suspension and only was detected when concentrated in the drying sample preparation process for SEM. These results indicate that with future filtration strategies, a consistent size distribution can be maintained across levels of hemoglobin inclusion. We also performed similar analyses for other silk fibroin particle formulations and present those results in Figure S4, Supporting Information.

2.2.2. Passive Encapsulation of Functional Human Hemoglobin Maintains O₂ Binding Capacity

To confirm we encapsulated hemoglobin into the particle matrix, we quantified hemoglobin incorporation (Figure 5ABC) and performed immunofluorescence microscopy to visualize hemoglobin incorporation (Figure 5D). Particles were made using a ferrous (oxygen binding) form of hemoglobin, referred to as HbA₀. Following the same methods described in Section 2.2.1., we then

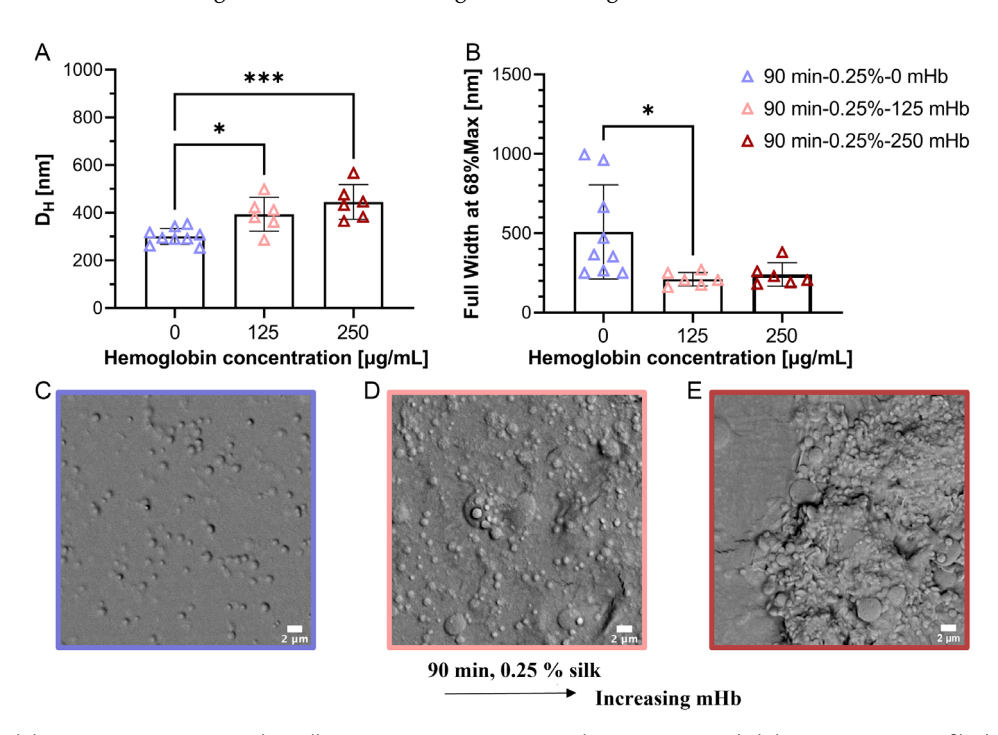


Figure 4. As hemoglobin concentration approaches silk concentration, average particle size increases slightly. A) Comparison of hydrodynamic diameter $(D_{\rm H})$ for 90 min-0.25%-X formulations as measured by DLS. B) Comparison of peak width at 68% of the maximum for 90 min-0.25%-X formulations, an assessment of dispersity. C) Representative SEM micrograph for 90 min-0.25%-0 mHb. D) Representative SEM micrograph for 90 min-0.25%-125 mHb. E) Representative SEM micrograph for 90 min-0.25%-250 mHb. Data shown are AVG \pm SD ($n \ge 6$). A one-way ANOVA with Tukey post hoc testing was performed. Statistical significance is shown as * $p \le 0.05$, ** $p \le 0.01$, **** $p \le 0.001$, **** $p \le 0.0001$.

and-conditions) on Wiley Online Library for rules of use; OA articles are governed by the applicable Creative Commons License

www.advancedsciencenews.com www.advnanobiomedres.com

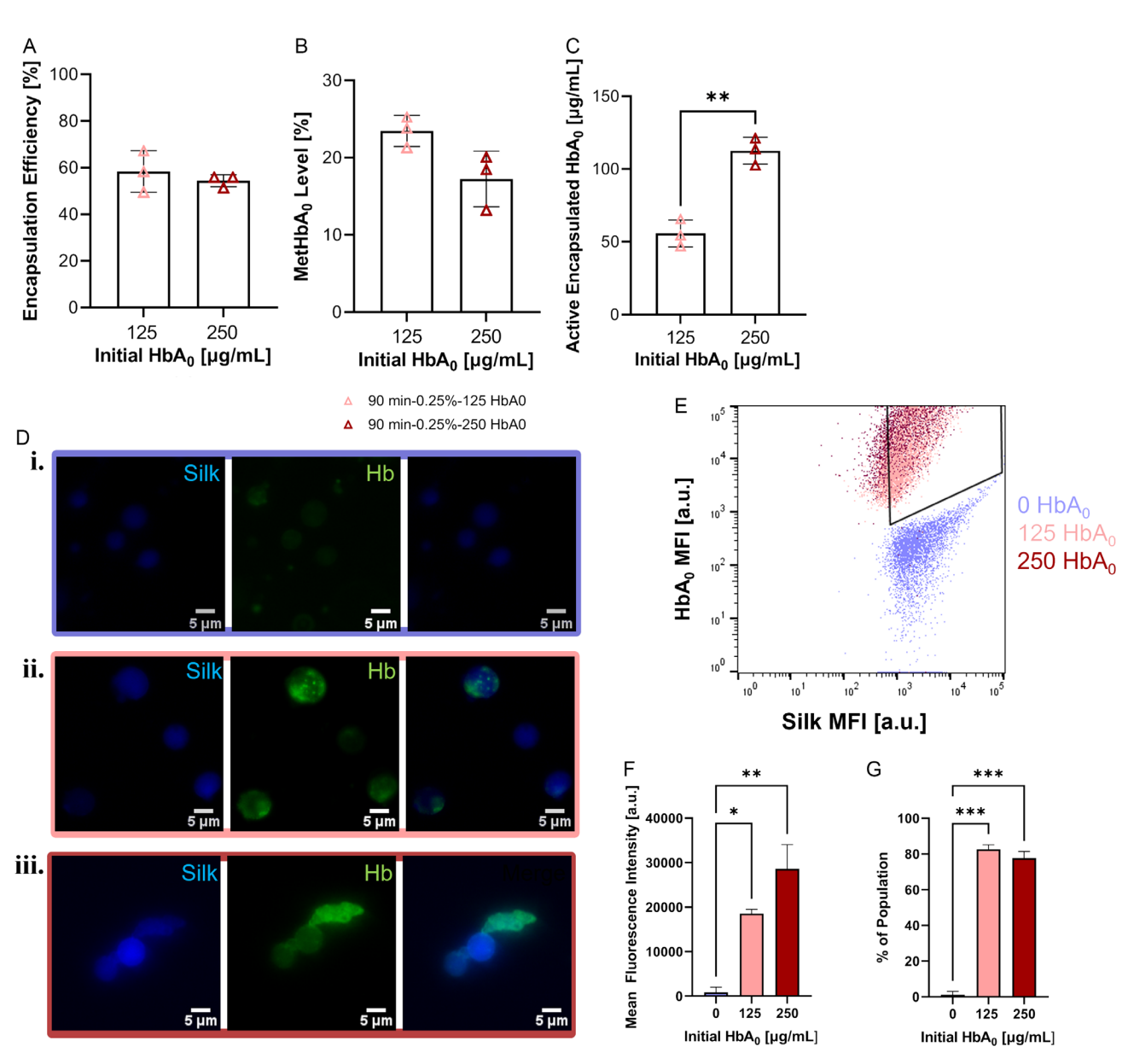


Figure 5. Functional hemoglobin is incorporated into silk particles. A) Hemoglobin encapsulation efficiency was determined for 90 min-0.25% w/v silk formulations with initial hemoglobin concentrations of 125 and 250 μ g mL⁻¹ using the cyanmethemoglobin method. B) The level of methemoglobin (an oxidized, nonoxygen binding form of hemoglobin) was determined for 90 min-0.25% w/v silk formulations with initial hemoglobin concentrations of 125 and 250 μ g mL⁻¹ using the cyanmethemoglobin method. C) Combining the results shown in (A), (B), we calculated the concentration of active (oxygen binding) hemoglobin present for 90 min-0.25% w/v silk formulations with initial hemoglobin concentrations of 125 and 250 μ g mL⁻¹. D) Fluorescent stain for hemoglobin in 90 min-1% w/v silk formulations with initial concentrations of i) 0, ii) 125 and, iii) 250 μ g mL⁻¹. Silk is shown in blue and hemoglobin is shown in green. E) Flow cytometry was also performed to assess association of hemoglobin to silk. Using the same antibodies used in the immunofluorescent imaging, 90 min-0.25% w/w with initial hemoglobin concentrations of 0, 125, and 250 μ g mL⁻¹ were analyzed. Samples were gated using FSC/SSC and negative controls (Supplemental Figure S11). A minimum of 5000 events per sample were collected. F) The mean fluorescence intensity (MFI) of hemoglobin was determined for populations with in the silk-hemoglobin gate shown in (E). G) The percent of the total population that fell within the silk-hemoglobin gate was determined. Data shown are AVG \pm SD (n = 3). A one-way ANOVA with Tukey post hoc testing was performed. Statistical significance is shown as $*p \le 0.05$, $***p \le 0.01$.

used a FITC-conjugated antibody with a human hemoglobin A target. In Figure 5D we show colocalization of the hemoglobin signal (green) with the silk fibroin particles signal (blue). We observe limited unspecific binding of the antibody (Figure 5D, i) and observe that with increasing initial HbA_0 concentrations,

Hb can agglomerate in the wall or on the edges of particles (Figure 5D, iii). When the silk is in excess relative to the hemoglobin, we observe disperse hemoglobin inclusion across the particle surface (Figure 5D, ii) In order to allow for visualization of hemoglobin signal, larger particles were formed and imaged



NANOBIOME RESEARCH

www.advancedsciencenews.com

www.advnanobiomedres.com

(Figure 5D). To understand hemoglobin encapsulation of the smaller particles (<1 µm), we utilized flow cytometry. Using the same staining mechanism, particles were analyzed for positive Hb signal (y-axis) and positive silk signal (x-axis) (Figure 5E). We quantified the mean fluorescence intensity (MFI) of this population and observed as hemoglobin concentration increased, so did signal intensity (Figure 5F). The percentage of total particle population that fell in the positive hemoglobin and silk gate was also analyzed and is shown in Figure 5G. Knowing that we can encapsulate mHb in the silk particle matrix, we then confirmed that our organic solvent free method maintains the gas binding capabilities of hemoglobin. To assess this, we encapsulated the ferrous form of hemoglobin (HbA₀) in the same particle formations and utilized the cyanmethemoglobin method and spectrophotometry to analyze both the overall hemoglobin encapsulation efficiency as well as the levels of methemoglobin (ferric, nonactive hemoglobin) present in the samples (Figure S7A,B, Supporting Information). We found that independent of the initial HbA₀ concentration efficiency remained constant at just under 60% (Figure 5A). This was further supported by finding the percent of initial hemoglobin that partitioned to the nonsilk phase during fabrication which averaged about 40% (Figure S10, Supporting Information). This shows that the mass balance of hemoglobin in the fabrication process is well balanced and we are losing very little during centrifugation steps. Taken together, these results suggest that we were on the maximum side of the level of encapsulation we can achieve.

To further investigate this, we performed the same experiment with increased initial HbA₀ concentrations and found that encapsulation efficiency continues to decline for increasing initial HbA₀concentrations (Figure S9A, Supporting Information). We then used the cyanmethemoglobin method to assess the level of methemoglobin in the samples (Figures S7B, Supporting Information). From here, the amount of total active hemoglobin was calculated from the initial HbA₀ concentration multiplied by the encapsulation efficiency, subtracting out the contribution of methemoglobin. We found that a maximum of 23% of encapsulated hemoglobin was in the ferric methemoglobin form (Figure 5B). Other research in the HBOC field has shown that methemoglobin levels around 10% allowed for substantial oxygenation of tissues. [65] Native RBCs in a healthy individual have levels of methemoglobin of only ≈1%, largely due to reductase enzymes allowing the methemoglobin to be reversed to its ferrous form. Some liposome based HBOCs have been able to nearly match the level of methemoglobin initially after formulation when freshly isolated hemoglobin from expired blood units are used. [24,66] We hypothesize that improved hemoglobin sourcing (initial hemoglobin methemoglobin content used in this study was \approx 12%) and timelines can further improve the level of methemoglobin we observe in our system. However, for applications not replacing more than 30% of the blood volume, methemoglobin levels of \approx 20% in HBOCs can be helpful in supporting nativeRBCs.^[65] We found that initial HbA₀ concentrations of 250 $\mu g \, m L^{-1}$ led to similar levels of $\approx 100 \, \mu g \, m L^{-1}$ active hemoglobin in both 90 min 0.25% w/v and 90 min 1% w/v formulations (Figure 5B and S8, Supporting Information). This is $\approx 1/1,000$ the concentration of hemoglobin in the blood of a healthy individual. This is a limitation to this system at present and future investigations utilizing stealth polymers to allow for ample concentration of the particle in suspension while maintaining stability is ongoing. However, there are some applications in which formulations with lower concentration HBOCs can be utilized for applications where supplementation, not full replacement, of RBCs is necessary. These clinical situations include blood loss related to trauma in a nonclinical setting (e.g., battlefield, car accident), blood loss in immune compromised patients where transfusion of human donor blood is suboptimal (e.g., post childbirth, during a pandemic), or situations where a patient is unable to receive a transfusion due to religious convictions.

2.3. Silk Particles Do Not Illicit Pro-Inflammatory Response in Macrophages

Finally, to analyze the potential utility sfHBOCs, we investigated how macrophages, important phagocytes of the innate immune system, respond to sfHBOCs in culture. Understanding the ability of our particles to alter expression of key markers in mouse macrophage-like cells will give insight into future experimental design as we move toward clinical translation of silk fibroin particle technologies. Macrophages are an important cell type to understand the behavior of with this technology because resident macrophages of the liver and spleen are responsible for the clearance of cell-free Hb, and for the clearance of particles or any foreign matter from circulation. In homeostatic conditions, cell-free hemoglobin is cleared by liver macrophages via a CD163 mediated uptake of hemoglobin-haptoglobin complexes. [67-69] In an ideal HBOC system, resident macrophages of the liver and spleen will be able to carry out this homeostatic function without being overwhelmed/stimulated by the carrier itself. Here we are describing a silk fibroin-based carrier, so it is important to understand the impact silk fibroin particles have on monocyte/ macrophage-like cells. Implanted neat silk fibroin materials have shown evidence of innate immune phagocytes infiltration at the site of implantation for up to 2 weeks via analysis of CD68 expression, suggesting only mild and acute inflammation, an important step in the tissue healing cascade. [49,70] Previous studies with silk fibroin particles engineered for IP delivery also show mild inflammatory response by macrophages via the monitoring of TNF- α both pre- and post-translation. [45,54,71] Here we observe limited activation of murine blood derived RAW 264.7 macrophages via the assessment of iNOS protein expressionin cultures that are stimulated twice over 72 h (Figure 6). This was observed for both neat silk particles as well as hemoglobin containing particles. When the percent of iNOS positive cells was normalized to the ground M0 control, all particle formulations but one resulted in a statistically similar decrease in iNOS expression and the only significant increase in iNOS positive cells was in the M1 positive control group. Additionally, if the percent of iNOS positive cells is normalized instead to the M1 control, we observe all particle conditions, like the anti-inflammatory (M2) control and M0 control, maintain a negative fold change from the positive control group (Figure S12, Supporting Information). Taken together, this assay demonstrates the potential of silk particles to be cleared effectively and safely via native processes without substantially impacting long term macrophage phenotype or activity.

and-conditions) on Wiley Online Library for rules of use; OA articles are governed by the applicable Creative Commons

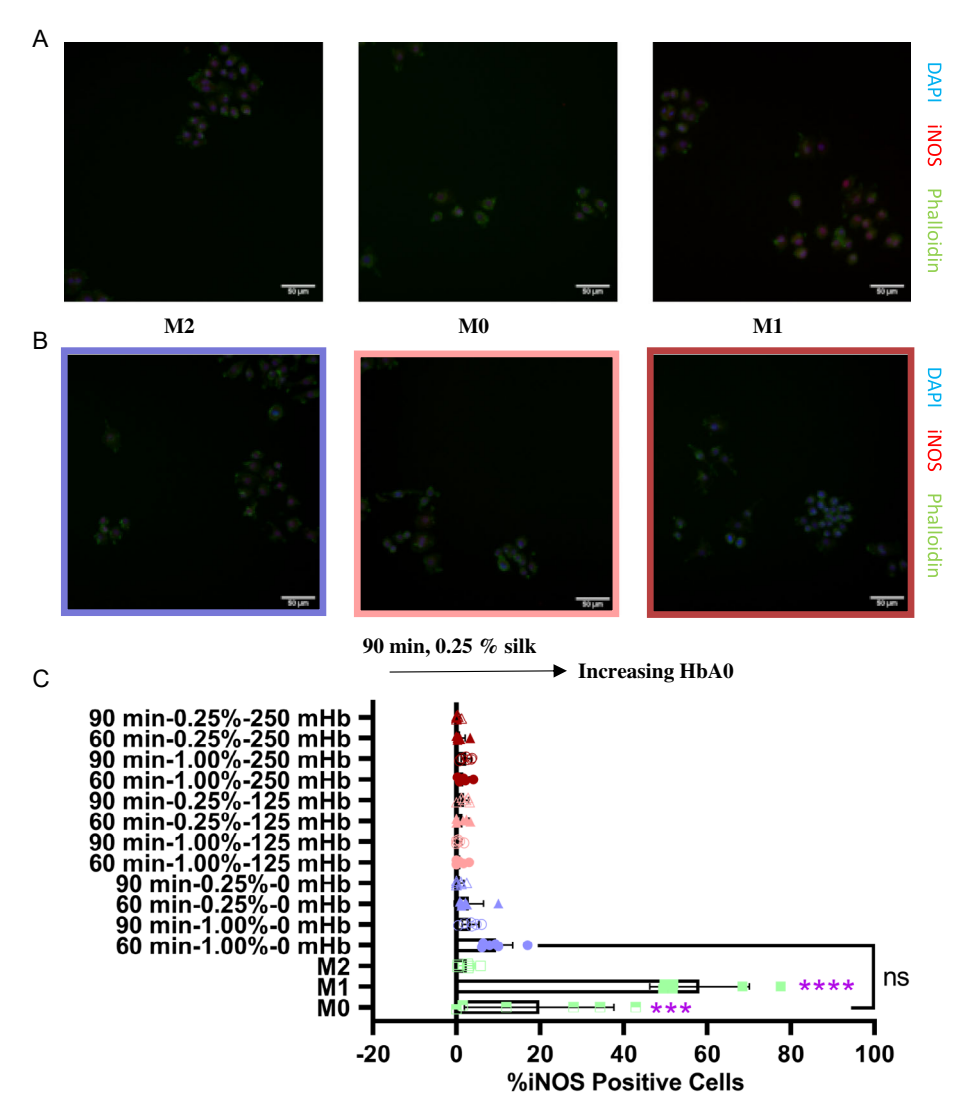


Figure 6. iNOS expression in RAW 264.7 is not significantly increased with particle incubation. A) Fluorescent images of negative (M2) ground (M0) and positive (M1) controls for iNOS (red) expression. Cells were also stained for nuclei (DAPI, blue), as well as spreading (Phalloidin, green). B) Fluorescent images for 90 min-0.25%- X HbA $_0$ formulations. iNOS (red), DAPI (blue), Phalloidin (green) C) Quantified percent of iNOS expressing cells is shown. Data represented as AVG \pm SD (n=6). A one-way ANOVA with Tukey post hoc testing was performed. Statistical significance is shown as * $p \le 0.05$, ** $p \le 0.01$, *** $p \le 0.001$, *** $p \le 0.001$.

3. Conclusion

The results of this work have leveraged the properties of silk fibroin, an all-natural and nonthrombogenic biopolymer, to engineer a nanoparticle system as a carrier for hemoglobin, generating a sfHBOC as an alternative delivery vehicle to the liposome-dominated field of HBOCs. The results of this study demonstrate that an aqueous processing method can yield control over particle size, achieving particles <500 nm in diameter with stable encapsulation of active hemoglobin (ability to bind O_2 based on oxidation state). These formulations do not elicit unwanted immune responses from macrophage-like cells in vitro.

Furthermore, the crystalline content in silk fibroin particles is critical for understanding the potential to include and stabilize

hemoglobin within these particles to create sfHBOCs. Proteins and biomolecules are stabilized within the crystalline domains of the silk protein, trapping the bioactive molecule in a stable confirmation even when the particles experience various hydration levels or temperatures. This feature of silk fibroin biomaterials is what makes this all-natural carrier system advantageous as a HBOC.

In conclusion, the sfHBOC has the potential to address the adverse reactions observed in early iterations of HBOCs. These findings hold significant promise for the development of an injectable HBOC that can address the limitations of current HBOCs and provide effective oxygen delivery in transfusion medicine and the treatment of diseases. Further research is needed to evaluate the safety and efficacy of sfHBOCs in vivo.

NANOBIOMED RESEARCH

www.advancedsciencenews.com www.advnanobiomedres.com

4. Experimental Section

Silk Solution Preparation: Silk fibroin was isolated from Bombyx mori cocoons as previously described. [50] Briefly, five grams of dime-size sections of silk cocoons were boiled to extract fibroin proteins from sericin proteins for 15, 30, 60, or 90 min in 2 L of 0.02 M aqueous sodium carbonate (Na₂CO₃) solution (Catalog No. 451 614, Sigma Aldrich, St. Louis, MO). Once degumming was complete, the fibroin mat was air-dried for a minimum of 48 h. The solid protein mat is then solubilized at 60 °C for 4 h in 9.3 M aqueous lithium bromide (LiBr) solution (Catalog No. 213 225, Sigma Aldrich, St. Louis, MO). This solution was then dialyzed against ultrapure water using 3.5 kDa MW cutoff dialysis membrane tubing (Spectrum Spectra/Por 3 RC Dialysis Membrane Tubing, 3,500 Dalton MWCO, Catalog No. 08-670-5C, ThermoFisher Scientific, Waltham, MA) over 48 h to remove ions. LiBr was considered to be fully removed when the conductivity falls below 5 uS cm-(DI Water k = 1-3 uS cm⁻¹). For silk used throughout this manuscript the conductivity was measured upon removal from dialysis and was 3.82 and 3.59 us cm⁻¹ for 60 and 90 min extracted silk, respectively. The solubilized, aqueous silk solution was then centrifuged ($4000 \times g$, 20 min, 4 °C) twice to remove any insoluble impurities. The concentration (weight/volume) is determined by drying a known volume of the silk solution at 60 °C and weighing the remaining solids. This protocol resulted in a 5%-7% weight per volume w/v silk fibroin solution. Silk solutions were stored at 4 °C for a maximum of 3 weeks prior to use in making particles.

Gel Electrophoresis: Silk molecular weight (MW) distributions after fiber degumming were visualized with sodium dodecyl sulfate polyacrylamide gel electrophoresis (SDS-PAGE). Samples of varied extraction times (15, 30, 60, and 90 min) and four batches of 60 min extracted silk were analyzed. For each sample 2 µg of solubilized silk protein was loaded into a NuPAGE 7% Tris-acetate gel (EA03585BOX, Invitrogen, Waltham, MA) under reducing conditions. 5 µL of a high molecular weight ladder (HiMark Pre-stained Protein Standard LC5699, Invitrogen) was loaded in lane 1 of each gel. Gels were loaded into an Invitrogen mini gel tank (A25977) and run with Bolt 1X MES SDS Running buffer (Life Technologies, Carlsbad, CA). Using a power ease 300 W (Life Technologies) power supply each gel was run at 100 V for 5 min and then the voltage was increased to 200 V for 23 min. The gels were stained with a Colloidal Blue staining kit (LC6025, Invitrogen) and then imaged on an Odyssey Fc (LI COR, Lincoln, NE) at 700 nm with a 30 s exposure time. The MW distributions of the solubilized silk samples were quantified with densitometric measurements along the length of each lane (Image Studio version 5.2, LI COR).

Silk and Silk-Hemoglobin Particle Preparation: Silk fibroin control particles are formed via a phase separation from polyvinyl alcohol (PVA) (P8136, Sigma Aldrich) modified from previous techniques. [50,51] Briefly. stock solutions of 5% w/v of silk and PVA are prepared. The silk and PVA were combined in a 1:4 weight ratio in a total volume of 5 mL. The resulting solution was then probe sonicated at 25% for 30 s. Post sonication, the solution was cast into a $100 \times 15 \text{ mm}$ petri dish. Once dried overnight, the plastic-like film is shaken for 30 min in 20 mL dI water to dissolve. The resulting solution is centrifuged $(4000 \times g, 20 \text{ min}, 4 ^{\circ}\text{C})$. The pellet containing silk particles was then resuspended in 5 mL of ultrapure water and sonicated at 15% for 15 s. In an effort to modulate the size of the particles, the extraction time of the silk used, and the silk concentration were varied as summarized in Table 1. A weight ratio of 1:4 silk: PVA was held constant across all conditions. Hemoglobin was passively encapsulated by combining the desired concentration of hemoglobin with silk solution prior to combining with PVA. For assessment of particle size and morphology, bovine hemoglobin (H2625, Sigma Aldrich), which was primarily in the ferric form was used (referred to as methemoglobin (mHb) throughout the manuscript, methemoglobin content >85%). For encapsulation and cell experiments a human hemoglobin in ferrous form was used (H0267, Sigma Aldrich, methemoglobin content \approx 12%), referred to as HbA₀ throughout manuscript.

Fourier Transform Infrared Spectroscopy: Quantification of the β-sheet content and other secondary protein structures in silk particles was performed using Fourier transform infrared spectroscopy (FTIR) analysis. Prior to FTIR analysis, particles were lyophilized at –80 °C and 0.160 mbar

for 2 days (FreeZone 12 L -84 °C Console Freeze Dryer, Labconco, Kansas City, MO). Spectra were collected with a Nicolet iS50 FTIR Spectrometer (ThermoFisher Scientific, Waltham, MA) (UF Nanoscale Research Facility), equipped with a microattenuated total reflections (microATR) germanium crystal and MCT/A detector. Each measurement consisted of 128 scans with a resolution of $4\,\mathrm{cm}^{-1}$ over wavenumbers ranging $4000-650\,\mathrm{cm}^{-1}$. Background spectra were collected using the same conditions and subtracted from each sample spectra. The amide I region (1590–1710 cm $^{-1}$) can be split into regions based on the protein secondary structure: $1605-1615\,\mathrm{cm}^{-1}$ as side chain/aggregated strands, $1616-1637\,\mathrm{cm}^{-1}$ and $1697-1703\,\mathrm{cm}^{-1}$ as β -sheet structure, $1638-1655\,\mathrm{cm}^{-1}$ as random coils, $1656-1662\,\mathrm{cm}^{-1}$ as α -helical bands, and $1663-1696\,\mathrm{cm}^{-1}$ as turns. For analysis the amide I region was deconvoluted to obtain relative amounts of respective secondary structures as detailed by Hu et al. $1000\,\mathrm{cm}^{-1}$ and $1000\,\mathrm{cm}^{-1}$ and $1000\,\mathrm{cm}^{-1}$ as convoluted to obtain relative amounts of respective secondary structures as detailed by Hu et al.

Nanoscale Computed Tomography: Assessment of internal particle morphology and detection of dense crystalline regions of silk was done through use of Nano-CT at the UF Nanoscale Research Facility. Particles were prepared using 60 min extracted silk at 1% w/v. The resulting particle solution was lyophilized (FreeZone 12 Liter –84 °C Console Freeze Dryer, Labconco, Kansas City, MO) for 48 h. The lyophilized particles were then imaged (v|tome|x m 240; General Electric) and analyzed using VGStudio Max.

Dynamic Light Scattering: The particle size and polydispersity of silk nanoparticle formulations in ultrapure water was determined at 25 °C by dynamic light scattering (DLS) using a Zetasizer Nano-ZS Malvern Instrument. The refractive indices of 1.33 for water and 1.60 for silk protein are used as had been done previously for silk materials and all measurements are conducted in triplicate (error not propagated). $^{[72]}$ In analysis of the dispersity of particle solutions, we determined the peak width at 68% lower than the peak maximum. This was done to represent a standard deviation since in a normal distribution 68% of the population falls within one standard deviation. $^{[73]}$

Scanning Electron Microscopy: 10 μ L of particle suspension in water was directly added to a ZEISS/LEO SEM Pin Stub Mount with an adhesive sticker, Ø12.7 mm \times 9 mm pin height (Catalog No. 16 202, Ted Pella, Inc., Redding, CA). The samples were then dried in a chemical hood for 48 h and sputter-coated with 10 nm of Au prior to imaging on a Phenom Pure benchtop SEM.

Estimation of Encapsulation Efficiency and Methemoglobin Level by UV-vis Spectroscopy: Spectrophotometric absorbance measurements were obtained using a NanoDrop One/One^c (ThermoFisher Scientific, Waltham MA). The total Hb and metHb (i.e., oxidized Hb in the Fe3+ valence state) concentrations were determined using the cyanmethemoglobin method. [74,75] To determine the total concentration of hemoglobin, 20% potassium ferricyanide K₃(Fe(CN)₆) (ThermoFisher Scientific, AC211095000) was added to samples and allowed to react for 3 min, converting all hemoglobin to methemoglobin. Then, 10% KCN (ThermoFisher Scientific, AAL1327322) was added to form cyanmethemoglobin with unique absorbance behavior. The absorbance was then measured at 540 nm. The final hemoglobin concentration was calculated as a dilution coefficient multiplied with the ratio of the absorbance and the extinction coefficient of methemoglobin at 540 nm [cm mM]⁻¹ (Figure S5A, Supporting Information). The methemoglobin levels of encapsulated hemoglobin were found using cyanmethemoglobin method and UV-vis.^[74,75] The absorbance of the sample was measured at 630 nm. Then a 1:1 KCN and PBS solution was added to samples. This converted methemoglobin to cyanomethemoglobin, which was absorbed at 630 nm. After a minimum of 3 min, the absorbance was read again at 630 nm. The concentration of methemoglobin can be calculated as a dilution coefficient multiplied by the ratio of the change in absorbance over the extinction coefficient for methemoglobin at 630 nm [cm mM]⁻¹ (Figure 5B).

Fluorescent Imaging of Hemoglobin: Hemoglobin encapsulation in silk particles was visualized using fluorescent microscopy. Samples were prepared with 90 min-1% silk and initial HbA0 (H0267, Sigma Aldrich) concentrations of 0, 125, and 250 $\mu g \, mL^{-1}$. Following particle formation, 100 μL of particle solution was placed in microcentrifuge tubes and combined with blocking media (5% donkey serum in 1% bovine serum



www.advancedsciencenews.com

www advnanobiomedres com

albumin (BSA) in PBS) and incubated at room temperature for a minimum of 4 h. After blocking, samples were washed three times with PBS with 0.1% tween (PBST) and then incubated overnight at 4 °C with a human hemoglobin-FITC conjugated antibody (Life Technologies, A80134F). Samples were washed three times with PBST prior to imaging on a Keyence BZ-X800 microscope.

Flow Cytometry Analysis: Samples were prepared with 90 min-0.25% silk or 90 min-1% silk, and initial HbA₀ (H0267, Sigma Aldrich) concentrations of 0, 125, and 250 µg mL⁻¹. Following particle formation, 1000 µL of particle solution was placed in microcentrifuge tubes and combined with blocking media (5% donkey serum in 1% bovine serum albumin (BSA) in PBS) and incubated at room temperature for a minimum of 4 h. After blocking, samples were washed three times with PBS with 0.1% tween (PBST) and then incubated overnight at 4°C with a human hemoglobin-FITC conjugated antibody (Life Technologies, A80134F). Samples were run on a Cytek Northern Lights (Fremont, CA). Controls of stained free hemoglobin, unstained free hemoglobin, unstained neat particles, and stained neat particles were all run to aid in gating the positive population. First, samples were gated for singlets using FSC and SSC. Then, a positive gate for hemoglobin intensity and silk intensity were drawn with a minimum positive value of 103 using the B2 and V2 fluorochrome peak channels. A minimum of 5000 events for each sample were collected. Analysis was completed using FlowJo (Ashland, OR)

RAW 264.7 Culture: The murine BALB/c derived RAW 264.7 cell line was obtained from ATCC (Manassas, Va). The cells were maintained in Dulbecco's Modified Eagle's Medium (DMEM) (Gibco) which was supplemented with 10% v/v fetal bovine serum (FBS) (Gibco) and 1% v/v $10\,000\,U\,mL^{-1}$ Penicillin–Streptomycin (15-140-122, Gibco). This base media formulation serves as the M0 control media. Cells were routinely subcultured every 3–4 days and maintained at 37 °C in 5% CO₂. Macrophage activations were assessed by seeding at 1.05×10^4 cells cm⁻¹ and allowing them to recover overnight. M1 stimulation media was M0 control media with 10 ng mL^{-1} IFN- γ (Peprotech) and 100 ng mL^{-1} Lipopolysaccharide (LPS) (SigmaAldrich) added. M2 stimulation media was M0 media with 40 ng mL^{-1} IL-4 (Peprotech) and 20 ng mL^{-1} IL-13 (Peprotech) added. Stimulation with M1 media, M2 media, and silk particles occurred 24 h after seeding. 250 µL of stimulation media was added to each well with unstimulated wells receiving M0 media. The wells stimulated with silk nanoparticles received 250 µL of M0 media supplemented with 50 µg of silk particles. 48 h poststimulation the media was changed using the same conditions as the first stimulation. This stimulation strategy resulted in 15 groups 72 h poststimulation: M0 (unstimulated), M1-Like, M2-Like, and the 12 silk nanoparticle formulations.

Immunostaining: An immunofluorescence assay was conducted to analyze the expression of iNOS (M1 marker) and cell spreading following the stimulation of RAW 264.7 cells. The 72 h poststimulation cells were fixed in 10% Phosphate buffered formalin for 15 min at room temperature and then washed three times with phosphate buffered saline (PBS). The cells were then permeabilized with 0.05% Triton-X-100 for 20 min at room temperature and washed three times with PBS. Following permeabilization each well was blocked for 5 h with 5% donkey serum in 1% bovine serum albumin (BSA) in PBS at room temperature. After blocking, wells were washed three times with PBS with 0.1% tween (PBST) and then incubated overnight at 4 °C with the anti-iNOS primary antibody (Rabbit polyclonal Antibody, PA5-1624, Invitrogen) at 0.002 ng mL^{-1} in 1% BSA in PBS. Secondary control wells were incubated with only 1% BSA in PBS. Following primary incubation, wells were washed three times with PBST prior to incubation with the antirabbit secondary antibody (A31572, Invitrogen) at 2.5 μ g mL⁻¹ and phalloidin at 16.7 μ g mL⁻¹ for 2 h at room temperature in the dark. DAPI (ThermoFisher Scientific) was added to each well at $5 \, \mu g \, m L^{-1}$ for $10 \, min$ in the dark. Wells were washed with PBST three times before adding 200 μL PBST to each well and fluorescent microscopy was conducted with the Keyence BZ-X800 microscope. iNOS expression in images was quantified using cell Profiler.

Statistical Methods: Experimental data were mainly expressed as mean \pm standard deviation (SD) with a minimum n=2. In the case of the gel electrophores is data were expressed as median \pm half of the inner quartile range (Figure 1). GraphPad Prism 8.4.1 (La Jolla, CA) was utilized to

analyze these data. Analysis was completed with appropriate-sized analysis of variance (ANOVA). If significance was found, Tukey post hoc testing was used for pairwise comparisons. Statistical significance was reported as *p < 0.05, **p < 0.01, ***p < 0.001, and ****p < 0.0001, with key features shown in the figures and full information provided in the supplement. Specifics on the statistical test, p values, and definition of n are all present in individual figure captions.

Supporting Information

Supporting Information is available from the Wiley Online Library or from the author.

Acknowledgements

The Stoppel lab would like to acknowledge the research scientists at the University of Florida Nanoscale Research Facility, especially Gary Scheiffele, Ph.D., for their assistance with using core equipment, such as the Nano-CT and FTIR. Additionally, support from Stoppel Lab University of Florida undergraduates in silk solution preparation, including Travis Truong, Hannah Bagnis, and Marina Fernandez-Campa. The authors also appreciate assistance from Dr. Yeongseon Jang and her PhD student Jackson Powers for the use of their Malvern DLS instrument. All authors would like to acknowledge support from the Department of Defense Congressionally Directed Medical Research Fund (W81XWH2110199). A.S.C. acknowledges support from the Chemical Engineering REU Site at the University of Florida (NSF EEC-1852111). N.A.D. was supported by a grant from the National Institutes of Health (NIH T35HL007489). M.O.P. acknowledges support from the National Science Foundation Graduate Research Fellowship (DGE-1842473). Any opinions, findings, and conclusions or recommendations expressed in this manuscript are those of the authors and do not necessarily reflect the views of the National Science Foundation, National Institutes of Health, or Department of Defense.

Conflict of Interest

Whitney L. Stoppel, Bruce D. Spiess, and Marisa O. Pacheco have a pending patent on this research.

Data Availability Statement

The data that support the findings of this study are available in the supplementary material of this article.

Keywords

biopolymers, microparticles, oxygen carrier, silk fibroin

Received: March 1, 2023 Revised: May 23, 2023 Published online: July 27, 2023

[1] S.-B. Catrina, X. Zheng, Diabetologia 2021, 64, 709.

- [3] J. Duret, J. Pottecher, P. Bouzat, J. Brun, A. Harrois, J. F. Payen, J. Duranteau, *Crit. Care* **2015**, *19*, 141.
- [4] K. Sun, Y. Xia, Curr. Opin. Hematol. 2013, 20, 215.

^[2] N. J. White, K. R. Ward, S. Pati, G. Strandenes, A. P. Cap, J. Trauma Acute Care Surg. 2017, 82, S41.

www.advancedsciencenews.com

www.advnanobiomedres.com

- [5] E. Rezoagli, M. Petrosino, P. Rebora, D. K. Menon, S. Mondello, D. J. Cooper, A. I. R. Maas, E. J. A. Wiegers, S. Galimberti, G. Citerio, C. Ackerlund, K. Amrein, N. Andelic, L. Andreassen, A. Anke, G. Audibert, P. Azouvi, M. L. Azzolini, R. Bartels, R. Beer, B.-M. Bellander, H. Benali, M. Berardino, L. Beretta, E. Begiri, M. Blaabjerg, S. B. Lund, C. Brorsson, A. Buki, M. Cabeleira, et al., Intensive Care Med. 2022, 48, 1709.
- [6] L. J. Dumont, J. A. Cancelas, L. A. Maes, N. Rugg, P. Whitley, L. Herschel, A. H. Siegal, Z. M. Szczepiorkowski, J. R. Hess, M. Zia, Transfusion 2015, 55, 485.
- [7] K. Czubak, A. Antosik, N. Cichon, H. M. Zbikowska, Redox Rep. 2017, 22 445
- [8] S. Zou, Transfus. Med. Rev. 2006, 20, 181.
- [9] R. O. Gilcher, S. McCombs, Curr. Opin. Hematol. 2005, 12, 503.
- [10] M. Haracic, S. Simmonds, U. Krausbauer, Transfus. Med. Hemother. 2003, 30, 37.
- [11] E. Miskeen, A. I. Omer Yahia, T. B. Eljack, H. K. Karar, J. Multidiscip. Healthcare 2021, 14, 3063.
- [12] B. Fahimnia, A. Jabbarzadeh, A. Ghavamifar, M. Bell, Int. J. Prod. Econ. 2017, 183, 700.
- [13] A. Sen Gupta, Shock 2019, 52 70.
- [14] E. M. Ketcham, C. B. Cairns, Ann. Emerg. Med. 1999, 33, 326.
- [15] J. E. Manning, L. M. Katz, M. R. Brownstein, L. B. Pearce, M. S. Gawryl, C. C. Baker, Shock 2000, 13 152.
- [16] M. Cao, Y. Zhao, H. He, R. Yue, L. Pan, H. Hu, Y. Ren, Q. Qin, X. Yi, T. Yin, L. Ma, D. Zhang, X. Huang, Front. Med. 2021, 8, 794561.
- [17] H. Sakai, Y. Masada, S. Takeoka, E. Tsuchida, J. Biochem. 2002, 131,
- [18] F. Meng, T. Kassa, S. Jana, F. Wood, X. Zhang, Y. Jia, F. D'Agnillo, A. I. Alayash, Bioconjugate Chem. 2018, 29, 1560.
- [19] H. Sarin, J. Angiogenes Res. 2010, 2, 14.
- [20] A. I. Alayash, Shock 2019, 52, 41.
- [21] F. Vallelian, P. W. Buehler, D. J. Schaer, Blood 2022, 140, 1837.
- [22] J. S. Jahr, A. S. Akha, R. J. Holtby, Curr. Drug Discovery Technol. 2012, 9, 158.
- [23] L. Kuang, Y. Zhu, Y. Wu, K. Tian, X. Peng, M. Xue, X. Xiang, B. Lau, F. C. Tzang, L. Liu, T. Li, Front. Pharmacol. 2021, 12,
- [24] C. T. Cuddington, S. R. Wolfe, D. A. Belcher, M. Allyn, A. Greenfield, X. Gu, R. Hickey, S. Lu, T. Salvi, A. F. Palmer, Biotechnol. Bioeng. 2022, 119, 3447.
- [25] C. R. Muller, A. T. Williams, C. Walser, A. M. Eaker, J. L. Sandoval, C. T. Cuddington, S. R. Wolfe, A. F. Palmer, P. Cabrales, Sci. Rep. 2022, 12, 20480.
- [26] A. D. Farcas, V. A. Toma, I. Roman, B. Sevastre, F. Scurtu, R. Silaghi-Dumitrescu, Bioinorg. Chem. Appl. 2020, 2020, 1096573.
- [27] A. T. Kawaguchi, D. Fukumoto, M. Haida, Y. Ogata, M. Yamano, H. Tsukada, Stroke 2007, 38, 1626.
- [28] H. Azuma, M. Fujihara, H. Sakai, J. Funct. Biomater. 2017, 8, 24.
- [29] S. Rameez, A. F. Palmer, Langmuir 2011, 27, 8829.
- [30] T. Kure, H. Sakai, ACS Biomater Sci Eng. 2021, 7, 2835.
- [31] V. Awasthi, V. R. Yadav, B. Goins, W. T. Phillips, J. Microencapsul. **2013**, *30*, 471.
- [32] H. Sakai, K. Sou, E. Tsuchida, Methods in Enzymology, Academic Press, Cambridge, MA 2009, pp. 363-84.
- [33] X. Gu, A. F. Palmer, ACS Appl. Nano Mater. 2022, 5 5670.
- [34] V. T. Rentko, L. B. Pearce, P. F. Moon-Massat, M. S. Gawryl, Blood Substitutes (Ed: RM Winslow), Academic Press, Oxford 2006, pp. 424-36.
- [35] K. Chen, T. J. Merkel, A. Pandya, M. E. Napier, J. C. Luft, W. Daniel, S. Sheiko, J. M. DeSimone, Biomacromolecules 2012, 13, 2748.
- [36] D. T. Pham, W. Tiyaboonchai, Drug Delivery 2020, 27, 431.

- [37] M. Zhao, Z. Qi, X. Tao, C. Newkirk, X. Hu, S. Lu, Int. J. Mol. Sci. 2021, 22, 4136.
- [38] A. Bandyopadhyay, S. K. Chowdhury, S. Dey, J. C. Moses, B. B. Mandal, J. Indian Inst. Sci. 2019, 99, 445.
- [39] J. A. Kluge, A. B. Li, B. T. Kahn, D. S. Michaud, F. G. Omenetto, D. L. Kaplan, Proc. Natl. Acad. Sci. 2016, 113, 5892.
- [40] A. B. Li, J. A. Kluge, N. A. Guziewicz, F. G. Omenetto, D. L. Kaplan, J. Control Release 2015, 219, 416.
- [41] K. Y. Lee, S. J. Kong, W. H. Park, W. S. Ha, I. C. Kwon, J. Biomater. Sci. Polym. Ed. 1998, 9, 905.
- [42] M. F. Maitz, C. Sperling, T. Wongpinyochit, M. Herklotz, C. Werner, F. P. Seib, Nanomedicine 2017, 13, 2633.
- [43] X. Hu, D. Kaplan, P. Cebe, Macromolecules 2008, 41, 3939.
- [44] S. A. L. Matthew, J. D. Totten, S. Phuagkhaopong, G. Egan, K. Witte, Y. Perrie, F. P. Seib, ACS Biomater. Sci. Eng. 2020, 6, 6748.
- [45] J. D. Totten, T. Wongpinyochit, J. Carrola, I. F. Duarte, F. P. Seib, ACS Appl. Mater. Interfaces 2019, 11, 14515.
- [46] A. Florczak, T. Deptuch, A. Lewandowska, K. Penderecka, E. Kramer, A. Marszalek, A. Mackiewicz, H. Dams-Kozlowska, J. Nanobiotechnol. 2020. 18. 177.
- [47] M. G. Montalban, J. M. Coburn, A. A. Lozano-Perez, J. L. Cenis, G. Villora, D. L. Kaplan, Nanomaterials 2018, 8, 126.
- [48] M. O. Pacheco, L. E. Eccles, N. A. Davies, J. Armada, A. S. Cakley, I. P. Kadambi, W. L. Stoppel, Front. Chem. Eng. 2022, 4, 1.
- [49] J. F. Jameson, M. O. Pacheco, E. C. Bender, N. M. Kotta, L. D. Black, D. L. Kaplan, J. M. Grasman, W. L. Stoppel, bioRxiv. 2022:2022.05.24.493207, https://doi.org/10.1101/2022.05.24.493207.
- [50] D. N. Rockwood, R. C. Preda, T. Yucel, X. Wang, M. L. Lovett, D. L. Kaplan, Nat. Protoc. 2011, 6, 1612.
- [51] X. Wang, T. Yucel, Q. Lu, X. Hu, D. L. Kaplan, Biomaterials 2010, 31, 1025
- [52] L. S. Wray, X. Hu, J. Gallego, I. Georgakoudi, F. G. Omenetto, D. Schmidt, D. L. Kaplan, J. Biomed. Mater. Res. B 2011, 99, 89.
- [53] B. P. Partlow, A. P. Tabatabai, G. G. Leisk, P. Cebe, D. L. Blair, D. L. Kaplan, Macromol. Biosci. 2016, 16, 666.
- [54] N. V. Montoya, R. Peterson, K. J. Ornell, D. R. Albrecht, J. M. Coburn, Molecules 2020, 25, 890.
- [55] H. Rahmani, A. Fattahi, K. Sadrjavadi, S. Khaledian, Y. Shokoohinia, Adv. Pharm. Bull. 2019, 9, 601.
- [56] S. A. L. Matthew, R. Rezwan, Y. Perrie, F. P. Seib, Molecules 2022, 27, 2368.
- [57] T. Wongpinyochit, B. F. Johnston, F. P. Seib, ACS Biomater. Sci. Eng. **2018**, 4, 942.
- [58] X. Hu, D. Kaplan, P. Cebe, Macromolecules 2006, 39, 6161.
- [59] B. Crivelli, S. Perteghella, E. Bari, M. Sorrenti, G. Tripodo, T. Chlapanidas, M. L. Torre, Soft Matter. 2018, 14, 546.
- [60] J. I. Solomun, J. D. Totten, T. Wongpinyochit, A. J. Florence, F. P. Seib, ACS Biomater. Sci. Eng. 2020, 6, 2796.
- [61] W. L. Stoppel, D. Hu, I. J. Domian, D. L. Kaplan, L. D. Black, Biomed. Mater. 2015, 10, 034105.
- [62] A. R. Reeves, K. L. Spiller, D. O. Freytes, G. Vunjak-Novakovic, D. L. Kaplan, Biomaterials 2015, 73, 272.
- [63] J. A. Stinson, C. R. Palmer, D. P. Miller, A. B. Li, K. Lightner, H. Jost, W. C. Weldon, M. S. Oberste, J. A. Kluge, K. M. Kosuda, Vaccine 2020, *38*, 1652.
- [64] M. Amirikia, S. M. A. Shariatzadeh, S. G. A. Jorsaraei, M. S. Mehranjani, Eur. Biophys. J. 2018, 47, 573.
- [65] R. Linberg, C. D. Conover, K. L. Shum, R. G. Shorr, Artif. Cells Blood Substitutes Immobilization Biotechnol. 1998, 26, 133.
- [66] U. Banerjee, S. Wolfe, Q. O'Boyle, C. Cuddington, A. F. Palmer, PLoS One 2022, 17, e0269939.



RESEARCH

www.advancedsciencenews.com www.advnanobiomedres.com

- [67] P. W. Buehler, B. Abraham, F. Vallelian, C. Linnemayr, C. P. Pereira, J. F. Cipollo, Y. Jia, M. Mikolajczyk, F. S. Boretti, G. Schoedon, A. I. Alayash, D. J. Schaer, *Blood* 2009, 113, 2578.
- [68] C. J. Munoz, I. S. Pires, J. H. Baek, P. W. Buehler, A. F. Palmer, P. Cabrales, Am. J. Physiol. Heart Circ. Physiol. 2020, 318, H1296.
- [69] M. J. Nielsen, C. B. Andersen, S. K. Moestrup, J. Biol. Chem. 2013, 288, 18834.
- [70] A. E. Thurber, F. G. Omenetto, D. L. Kaplan, Biomaterials 2015, 71, 145.
- [71] T. Wongpinyochit, P. Uhlmann, A. J. Urquhart, F. P. Seib, *Biomacromolecules* **2015**, *16*, 3712.
- [72] T. Wongpinyochit, B. F. Johnston, F. P. Seib, J. Vis. Exp. 2016, 116, e54669.
- [73] G. Cumming, J. Williams, F. Fidler, Understanding Stat. 2004, 3, 299.
- [74] R. D. Whitehead Jr., Z. Mei, C. Mapango, M. E. D. Jefferds, Ann. N. Y. Acad. Sci. 2019, 1450, 147.
- [75] S. Rameez, H. Alosta, A. F. Palmer, Bioconjug. Chem. 2008, 19, 1025.